Article

Dominant s-Process Nucleosynthesis Confirmed by Barium Isotopic Ratios in the CEMP-rs Star TYC 6044-714-1

Riano E. Giribaldi * and Laura Magrini

Posted Date: 4 March 2026

doi: 10.20944/preprints202603.0357.v1

Keywords: CEMP-s stars; CEMP-rs stars; s-process; i-process; high-resolution spectroscopy; abundances; isotope ratios; nucleosynthesis

Article

Dominant s-Process Nucleosynthesis Confirmed by Barium Isotopic Ratios in the CEMP-rs Star TYC 6044-714-1

Riano E. Giribaldi * and Laura Magrini

INAF – Osservatorio Astrofisico di Arcetri, Largo E. Fermi 5, 50125 Firenze, Italy
* Correspondence: rianoesc@gmail.com or riano.escategiribaldi@inaf.it

Abstract

CEMP-rs stars are often interpreted as signatures of intermediate (i-) process nucleosynthesis during early AGB evolution, yet no observed pattern has been shown to favor the i-process over a simple r+s combination. We present a new analysis of TYC 6044-714-1 based on high-resolution UVES spectra and state-of-the-art 1D and 3D non-LTE modelling, deriving precise atmospheric parameters, elemental abundances, and barium isotopic ratios. Modelling of the Ba II 4934 Å line indicates that 86% of barium originates from the s-process, while the derived [Ba/Eu] = 0.25 dex further supports s-process dominance.

Keywords: CEMP-s stars; CEMP-rs stars; s-process; i-process; high-resolution spectroscopy; abundances; isotope ratios; nucleosynthesis

---

1. Introduction

The production of elements heavier than iron is governed by neutron-capture processes, traditionally classified as the slow (s-) and rapid (r-). Abundance heavy element patterns of several Carbon-Enhanced Metal-Poor (CEMP) stars [1] are difficult to reproduce by a simple combination of these two channels. This has motivated the consideration of an intermediate neutron-capture process (i-process), operating at neutron densities between those of the s- and r-processes [2]. CEMP stars are prime laboratories for testing this scenario. Yet distinguishing between a genuine i-process signature and a mixture of s- and r-process contributions remains challenging. Differences between theoretical heavy-element patterns often do not exceed ∼0.3 dex, requiring highly accurate abundance determinations. This task is complicated by uncertainties in atmospheric parameters, the limited availability of realistic 3D non-LTE line formation models, and spectral blending from carbon-bearing molecules in CEMP giants.

Standard 1D LTE methods are known to introduce significant biases in very metal-poor stars [3,4] —especially in giants, affecting both stellar parameters and derived abundances. While 1D NLTE corrections are available for some elements, their reliability remains uncertain. These modelling limitations directly impact the interpretation of neutron-capture diagnostics and the inferred nucleosynthetic origin. In this context, TYC 6044-714-1 provides an excellent test case. This characterised CEMP-rs star [5] offers a valuable opportunity to put constrains on the r+s- and i-process hypothesis under state-of-the-art modelling assumptions.

2. Observations and Stellar Parameters

TYC 6044-714-1 was observed with UVES [6] at the ESO VLT. A co-added spectra covering the blue and red spectral regions with resolution of $R \sim 70\,000$ and signal-to-noise ratios (S/N) of ∼140 in the blue and ∼430 in the red was acquired. We derived atmospheric parameters adopting the TITAN benchmark star HD 186478 [4] as reference, which also has a UVES archival spectrum. The spectra of

 doi:10.20944/preprints202603.0357.v1

both stars were processed and analysed following the same procedure to ensure a fully differential approach. Effective temperature ($T_{\rm eff}$= 4810 ± 41 K) was derived by fitting the wings of the Hα and Hβ Balmer lines using 3D non-LTE synthetic grids [9] as with the normalization-fitting method [4,7,8]. Surface gravity (log g= 1.70 ± 0.15 dex), metallicity ([Fe/H] = −2.17 ± 0.05 dex), and microturbulence (v_{mic} = 1.82 ± 0.04 km/s) were derived from Fe lines assuming 1D non-LTE line formation [12,13], using Turbospectrum [10] with MARCS model atmospheres [11]. A strictly differential analysis relative to HD 186478 was adopted to minimise systematic uncertainties. Microturbulence was constrained by requiring the absence of trends between Fe abundance and reduced equivalent width, excluding saturated lines. The final atmospheric parameters place TYC 6044-714-1 among metal-poor giants with properties closely matching those of the reference star.

3. Element Abundances and Barium Isotopic Fraction

Elemental abundances were derived by spectral synthesis using Turbospectrum. Table 2 list our determinations. Magnesium was determined from the 5528 and 5711 Å lines under 1D non-LTE adopting the departure coefficients in [14] applying the method in [27] (see Figure A1 in the Appendix). Carbon and nitrogen abundances are crucial for modelling lines in the blue spectral region (i.e Eu at 4129 and 4205 Å), as their molecular features contribute significant blending. Carbon abundance was derived from C I lines at 5082 and 5380 Å, and the Swan $^{12}C_2$ band at 5140–5166 Å (see Figure A2 in the Appendix). Nitrogen abundance was determined by modelling the CN molecular bands in the 3556–3590 Å and 3787–3812 Å regions (see Figure A3 in the Appendix). The ^{12}C/^{13}C ratio was measured from molecular features in the band at 4155-4240 Å. The iterative procedure ensured convergence of CNO, Mg, and Fe abundances.

Barium abundance was obtained from the subordinate lines at 6141 and 6496 Å as in [15], using the accurate oscillator strengths log gf = −0.070 and log gf = −0.365, respectively, from Table 1 of [18], which are derived from the transition probabilities in [25,26]. This atomic data was used successfully by [18] to recover the canonic solar abundance A(Ba) = 2.18 ± 0.08 dex [28] under 1D LTE, and to demonstrate that, for the solar case, 3D non-LTE corrections are negligible, while 1D non-LTE underestimates the abundance by ∼0.20 dex.

Similar to the solar case, our tests on TYC 6044-714-1 indicate that 1D LTE yield abundances consistent with 3D non-LTE corrections[1] based on the CO^{5}BOLD model atmosphere grids [16,17] and the model atom in [18]. On the other hand, 1D non-LTE tends to underestimate A(Ba) by ∼0.35 dex. This is exposed in Figures 1 and 2. The left panels show the fits under 1D LTE; and display 1D non-LTE line profiles of the same abundances, indicating that the latter would certainly require lower abundances to fit the observational lines. The right panels of the figures show the interpolations of the 3D non-LTE correction grids. This diagnostic is crucial for determining isotopic ratios through modelling of the Ba II resonance line at 4934 Å, as the Ba abundance –along the microturbulence– has the strongest influence on assessing the relative contributions of the s- and r-processes [15].

We fitted the 4934 Å resonance line using the hyperfine-structure (HFS) components and isotopic fractions listed in Tables B.1 and 5 of [15], adopting a 1D non-LTE approach with the departure coefficients from [18]. 1D non-LTE is necessary for modelling this resonance line, as demonstrated by extensive tests on metal-poor giants (Giribaldi et al., submitted), where 1D LTE syntheses produce profiles that are systematically too shallow to reproduce the observed spectra. Figure 3 shows that the observed line is best reproduced by a synthetic profile with an 86% s-process contribution: ^{134}Ba = 0.0246, ^{135}Ba = 0.0740, ^{136}Ba = 0.0808, ^{137}Ba = 0.1278, ^{138}Ba = 0.6928. Since the r- and i-process profiles are nearly indistinguishable, the remaining 14% of Ba may arise from either process or a mixture of both.

[1] https://www.chetec-infra.eu/3dnlte/abundance-corrections/barium/

Preprints.org (www.preprints.org) | NOT PEER-REVIEWED | Posted: 4 March 2026 doi:10.20944/preprints202603.0357.v1

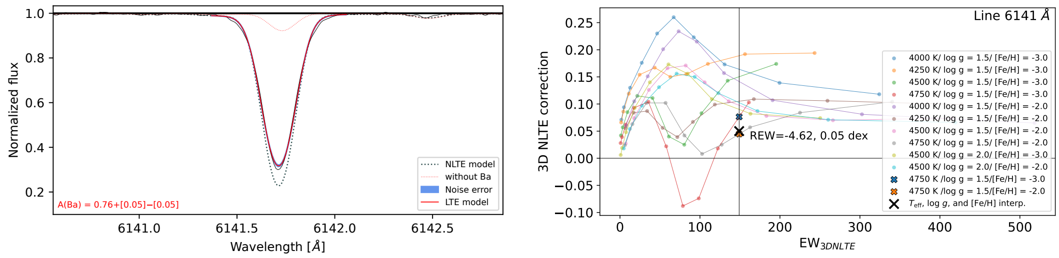

Figure 1. *Left panel:* Fit of the line at 6141 Å under 1D LTE. A 1D non-LTE line profile with the same determined abundance is shown by the dashed dark line. *Right panel:* Interpolation of the grid of 3D non-LTE Ba abundance corrections. Circles show the tabulated grid values, with stellar parameters indicated in the legend. Solid lines of matching colours represent linear interpolations between grid points. Crosses mark values interpolated in T_{eff} and log g, while the black cross corresponds to interpolation in T_{eff}, log g, and [Fe/H]. The figure also reports the line's reduced equivalent width (REW) and the resulting 3D NLTE correction.

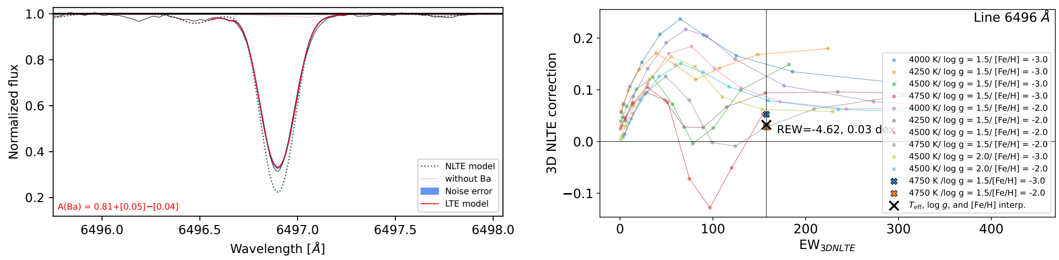

Figure 2. Similar to Figure 1 but for the line at 6496 Å.

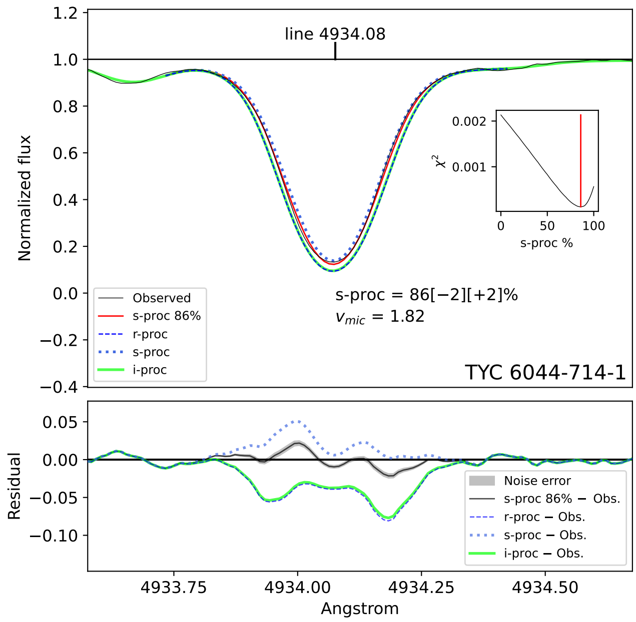

Figure 3. Fit of the Ba resonance line at λ4934 Å. Top panel: The observed profile is shown in black, and the best-fitting synthetic profile in red. The corresponding s-process percentage and its uncertainty (from spectral noise) are indicated in the plot. Additional synthetic profiles with the isotopic ratios listed in Table 5 in [15] are included as labelled in the legend. The inset displays the χ^2 distribution of the fits; the bar marks the s-process fraction corresponding to the minimum χ^2. Bottom panel: The black curve shows the residuals (best fit minus observation), with the grey shaded region indicating the flux uncertainty due to noise. Residuals for the r-, s-, and i-process profiles relative to the observed spectrum are plotted using the same line styles as in the top panel.

We derived the europium abundance from the 4129 and 4205 Å lines using 1D non-LTE modelling with the departure coefficients of [19]. Hyperfine-structure components were adopted from [29], and

Preprints.org (www.preprints.org) | NOT PEER-REVIEWED | Posted: 4 March 2026 doi:10.20944/preprints202603.0357.v1

the isotopic fractions from Table 1. Figure 4 shows that, for both transitions, the r- and i-process synthetic profiles are nearly indistinguishable. Therefore, despite the high quality of the spectrum, these Eu lines do not provide a diagnostic power comparable to that of the Ba resonance line.

Table 1. Europium isotopic fractions.

Process	^{151}Eu	^{153}Eu
Slow	0.4673	0.5327
Rapid	0.5008	0.4992
Intermediate	0.5221	0.4779

Notes. Quantities related the r-process are inferred from [30]. Quantities related to the s-process and i-process are inferred from a model of $1.5M_{\odot}$ with [Fe/H] $= -2.27$ dex (Giribaldi et al. submitted).

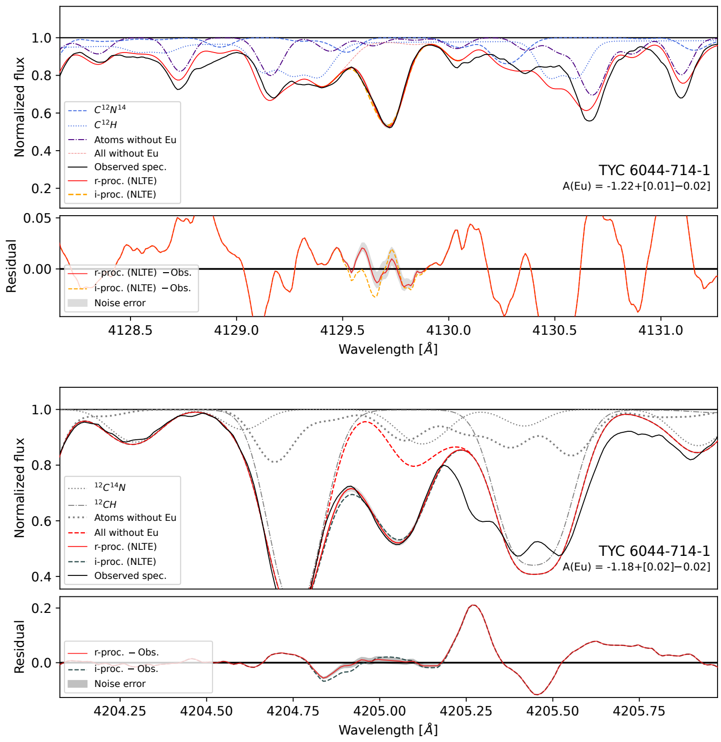

Figure 4. *Top panel:* Fit of the line at 4129 Å. Line profiles from the r- and i-processes from the isotopes fractions in Table 1 are represented in different colours as indicated in the legends. CN and CH molecule features are also plotted. *Bottom panel:* Similar to top pandl but for the line at 4205 Å.

Table 2. Element abundances.

Element	A(X)	[X/Fe]
C I	7.30 ± 0.06	1.00
$^{12}C_2$	7.25 ± 0.07	0.98
$^{12}C/^{13}C$	19	—
Mg	5.66 ± 0.04	5.28
Fe	5.28 ± 0.05	—
Ba	0.79 ± 0.10	0.70
Eu	-0.19 ± 0.08	0.45

Notes. A(X) indicates that for a given element X, the logarithmic absolute abundance is defined as the number of atoms of element X per 10^{12} hydrogen atoms, log ϵ(X) = A(X) $\equiv \log_{10}(NX/NH) + 12.0$. [X/Fe] indicates a logarithmic scale of A(X) relative that of iron A(Fe) relative to the Sun. For all elements except Mg and Fe, the solar canonical values of [28] were adopted. For Mg, the solar A(Mg) = 7.55 of [31] was adopted.

4. Conclusions

We derived accurate and precise abundances of C, Mg, Fe, Ba, and Eu for the CEMP star TYC 6044-714-1 using accurately determined atmospheric parameters and state-of-the-art line-profile modelling.

The barium isotopic fractions were inferred from the 4934 Å resonance line, adopting a well-constrained Ba abundance based on validated oscillator strengths and supported by prototype 3D non-LTE corrections. Our results indicate that the majority of the barium (86%) was synthesized by the s-process, while the remaining fraction may originate from the r-process, the i-process, or a combination of both. We derive [Ba/Eu] = 0.25 dex, consistent with observational signatures of s-process dominance (e.g., [32]), as negative [Ba/Eu] values are associated with stars with material dominated by the r-process (e.g., [33]).

Author Contributions: The authors contributed equally to this work.

Funding: R.E.G. and L.M. acknowledge support from INAF through the Large Grants EPOCH and WST, funding for the WEAVE project, the Mini-Grants Checs (1.05.23.04.02), and financial support under the National Recovery and Resilience Plan (PNRR), Mission 4, Component 2, Investment 1.1, Call for tender No. 104 published on 2 February 2022 by the Italian Ministry of University and Research (MUR), funded by the European Union – NextGenerationEU, through the Project 'Cosmic POT' (Grant Assignment Decree No. 2022X4TM3H, MUR).

Acknowledgments: This work is based on observations made with ESO Telescopes at the La Silla Paranal Observatory under programme IDs 114.27JT.001 or 0114.B-0030(A) and 165.N-0276(A). The 3D NLTE corrections of Ba used in this work were provided by the ChETEC-INFRA project (EU project no. 101008324), task 5.1. This research used Astropy,[2] a community-developed core Python package for Astronomy. This work presents results from the European Space Agency (ESA) space mission Gaia. Gaia data are processed by the Gaia Data Processing and Analysis Consortium (DPAC). Funding for the DPAC is provided by national institutions, in particular the institutions participating in the Gaia MultiLateral Agreement (MLA). The Gaia mission website is https://www.cosmos.esa.int/gaia. The Gaia archive website is https://archives.esac.esa.int/gaia.

Conflicts of Interest: The authors declare no conflicts of interest.

Abbreviations

The following abbreviations are used in this manuscript:

CEMP	Carbon Enhanced Metal-Poor
VLT	Very Large Telescope
UVES	Ultraviolet and Visual Echelle Spectrograph
LTE	Local Thermodynamic Equilibrium
3D	Three-dimensional hydrodynamic
HFS	Hyperfine Structure

Appendix A

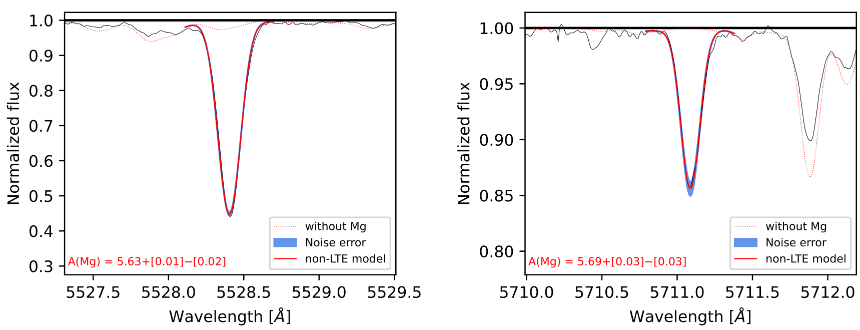

Figure A1. Fits of the Mg lines.

[2] http://www.astropy.org

 doi:10.20944/preprints202603.0357.v1

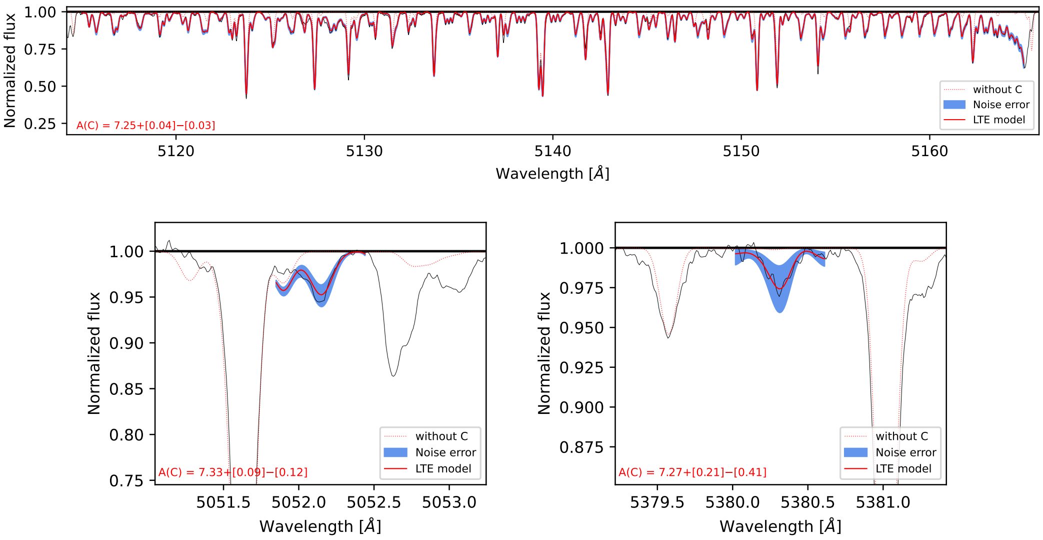

Figure A2. Fits of the Swan band $^{12}C_2$ *(top panel)* and the atomic lines *(bottom panels)*.

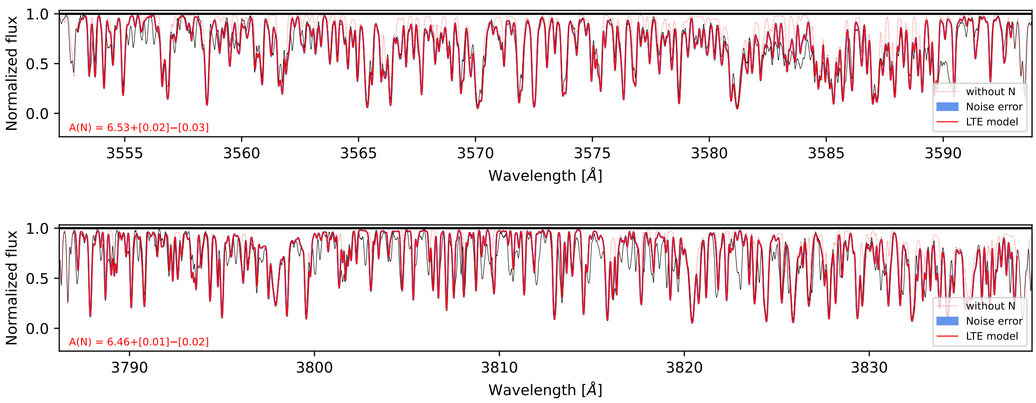

Figure A3. Fits of CN bands.

References

1. Beers, T. and Christlieb, N. The Discovery and Analysis of Very Metal-Poor Stars in the Galaxy. *ARA&A* **2005**, *43*, 531.
2. Cowan, J.J. and Rose, W.K. Production of ^{14}C and neutrons in red giants. *ApJ* **1977**, *212*, 149.
3. Ruchti, G.R.; Bergemann, M.; Serenelli, A.; Casagrande, L.; Lind, K. Unveiling systematic biases in the 1D LTE excitation-ionization balance of Fe for FGK stars: A novel approach to determination of stellar parameters. *Mon. Not. R. Astron. Soc.* **2013**, *429*, 126–134. https://doi.org/10.1093/mnras/sts319.
4. Giribaldi, R.E.; Van Eck, S.; Merle, T.; Jorissen, A.; Krynski, P.; Planquart, L.; Valentini, M.; Chiappini, C.; Van Winckel, H. TITANS metal-poor reference stars. II. Red giants and CEMP stars. *A&A* **2023**, *679*, A110. https://doi.org/10.1051/0004-6361/202347208.
5. Gull, M.; Frebel, A.; Cain, M.G.; Placco, V.M.; Ji, A.P.; Abate, C.; Ezzeddine, R.; Karakas, A.I.; Hansen, T.T.; Sakari, C.; Holmbeck, E.M.; Santucci, R.M.; Casey, A.R.; Beers, T.C. The R-Process Alliance: Discovery of the First Metal-poor Star with a Combined r- and s-process Element Signature. *ApJ* **2018**, *862*, 174. https://doi.org/10.3847/1538-4357/aacbc3.
6. Dekker, H. et al. Design, construction, and performance of UVES, the echelle spectrograph for the UT2 Kueyen Telescope at the ESO Paranal Observatory. *SPIE* **2000**, *4008*, 534-545.
7. Giribaldi, R.E.; da Silva, A.R.; Smiljanic, R.; Cornejo Espinoza, D. TITANS metal-poor reference stars. I. Accurate effective temperatures and surface gravities for dwarfs and subgiants from 3D non-LTE Hα profiles and Gaia parallaxes. *Astron. Astrophys.* **2021**, *650*, A194. https://doi.org/10.1051/0004-6361/202140751.
8. Giribaldi, R.E.; Ubaldo-Melo, M.L.; Porto de Mello, G.F.; Pasquini, L.; Ludwig, H.-G.; Ulmer-Moll, S.; Lorenzo-Oliveira, D. Accurate effective temperature from Hα profiles. *Astron. Astrophys.* **2019**, *624*, A10. .

9. Amarsi, A.M.; Nordlander, T.; Barklem, P.S.; Asplund, M.; Collet, R.; Lind, K. Effective temperature determinations of late-type stars based on 3D non-LTE Balmer line formation. *Astron. Astrophys.* **2018**, *615*, A139. .
10. Gerber, J.M.; Magg, E.; Plez, B.; Bergemann, M.; Heiter, U.; Olander, T.; Hoppe, R. Non-LTE radiative transfer with Turbospectrum. *Astron. Astrophys.* **2023**, *669*, A43. .
11. Gustafsson, B.; Edvardsson, B.; Eriksson, K.; Jørgensen, U.G.; Nordlund, Å.; Plez, B. A grid of MARCS model atmospheres for late-type stars. I. Methods and general properties. *Astron. Astrophys.* **2008**, *486*, 951–970. .
12. Bergemann, M.; Lind, K.; Collet, R.; Magic, Z.; Asplund, M. Non-LTE line formation of Fe in late-type stars—I. Standard stars with 1D and <3D> model atmospheres. *Mon. Not. R. Astron. Soc.* **2012**, *427*, 27–49. .
13. Semenova, E.; Bergemann, M.; Deal, M.; Serenelli, A.; Hansen, C.J.; Gallagher, A.J.; Bayo, A.; Bensby, T.; Bragaglia, A.; Carraro, G.; Morbidelli, L.; Pancino, E.; Smiljanic, R. The Gaia-ESO survey: 3D NLTE abundances in the open cluster NGC 2420 suggest atomic diffusion and turbulent mixing are at the origin of chemical abundance variations. *Astron. Astrophys.* **2020**, *643*, A164. .
14. Bergemann, M.; Collet, R.; Amarsi, A.M.; Kovalev, M.; Ruchti, G.; Magic, Z. Non-local Thermodynamic Equilibrium Stellar Spectroscopy with 1D and <3D> Models. I. Methods and Application to Magnesium Abundances in Standard Stars. *Astrophys. J.* **2017**, *847*, 15. https://doi.org/10.3847/1538-4357/aa88cb.
15. Giribaldi, R.E.; Magrini, L.; Schiappacasse-Ulloa, J.; Randich, S.; Merle, T. Barium isotopic ratios in metal-poor stars: Calibrating the method with globular clusters: I. Dwarf and giant stars in NGC 6752. *A&A* **2025**, *702*, A65. https://doi.org/10.1051/0004-6361/202556407.
16. Freytag, B.; Steffen, M.; Ludwig, H.-G.; Wedemeyer-Böhm, S.; Schaffenberger, W.; Steiner, O. Simulations of stellar convection with CO5BOLD. *J. Comput. Phys.* **2012**, *231*, 919–959. https://doi.org/10.1016/j.jcp.2011.09.026.
17. Ludwig, H.-G.; Caffau, E.; Steffen, M.; Freytag, B.; Bonifacio, P.; Kučinskas, A. The CIFIST 3D model atmosphere grid. *Mem. Soc. Astron. Ital.* **2009**, *80*, 711. https://doi.org/10.48550/arXiv.0908.4496.
18. Gallagher, A.J.; Bergemann, M.; Collet, R.; Plez, B.; Leenaarts, J.; Carlsson, M.; Yakovleva, S.A.; Belyaev, A.K. Observational constraints on the origin of the elements. II. 3D non-LTE formation of Ba II lines in the solar atmosphere. *Astron. Astrophys.* **2020**, *634*, A55. https://doi.org/10.1051/0004-6361/201936104.
19. Storm, N.; Barklem, P.S.; Yakovleva, S.A.; Belyaev, A.K.; Palmeri, P.; Quinet, P.; Lodders, K.; Bergemann, M.; Hoppe, R. 3D NLTE modelling of Y and Eu. Centre-to-limb variation and solar abundances. *Astron. Astrophys.* **2024**, *683*, A200. https://doi.org/10.1051/0004-6361/202348971.
20. Masseron, T.; Johnson, J.A.; Plez, B.; van Eck, S.; Primas, F.; Goriely, S.; Jorissen, A. A holistic approach to carbon-enhanced metal-poor stars. *Astron. Astrophys.* **2010**, *509*, A93. https://doi.org/10.1051/0004-6361/200911744.
21. Bisterzo, S.; Gallino, R.; Straniero, O.; Cristallo, S.; Käppeler, F. s-Process in low-metallicity stars - I. Theoretical predictions. *Mon. Not. R. Astron. Soc.* **2010**, *404*, 1529–1544. https://doi.org/10.1111/j.1365-2966.2010.16369.x.
22. Straniero, O.; Gallino, R.; Cristallo, S. s process in low-mass asymptotic giant branch stars. *Nucl. Phys. A* **2006**, *777*, 311–339. https://doi.org/10.1016/j.nuclphysa.2005.01.011.
23. Cristallo, S.; Straniero, O.; Gallino, R.; Piersanti, L.; Domínguez, I.; Lederer, M.T. Evolution, nucleosynthesis, and yields of low-mass asymptotic giant branch stars at different metallicities. *Astrophys. J.* **2009**, *696*, 797–820. https://doi.org/10.1088/0004-637X/696/1/797.
24. Vescovi, D.; Cristallo, S.; Palmerini, S.; Abia, C.; Busso, M. Magnetic-buoyancy-induced mixing in AGB stars: Fluorine nucleosynthesis at different metallicities. *Astron. Astrophys.* **2021**, *652*, A100. https://doi.org/10.1051/0004-6361/202141173.
25. Dutta, T.; de Munshi, D.; Yum, D.; Rebhi, R.; Mukherjee, M. An exacting transition probability measurement—A direct test of atomic many-body theories. *Sci. Rep.* **2016**, *6*, 29772. https://doi.org/10.1038/srep29772.
26. De Munshi, D.; Dutta, T.; Rebhi, R.; Mukherjee, M. Precision measurement of branching fractions of $^{138}Ba^{+}$: Testing many-body theories below the 1% level. *Phys. Rev. A* **2015**, *91*, 040501. https://doi.org/10.1103/PhysRevA.91.040501.
27. Giribaldi, R.E.; Magrini, L.; Rossi, M.; Amarsi, A.M.; Romano, D.; Massari, D. The most metal-poor tail of the Galactic halo: Hypothesis for its origin from precise spectral analysis. *Astron. Astrophys.* **2025**, *698*, A11. https://doi.org/10.1051/0004-6361/202453470.
28. Asplund, M.; Grevesse, N.; Sauval, A.J.; Scott, P. The Chemical Composition of the Sun. *Annu. Rev. Astron. Astrophys.* **2009**, *47*, 481–522. https://doi.org/10.1146/annurev.astro.46.060407.145222.

doi:10.20944/preprints202603.0357.v1

29. da Silva, A.R.; Smiljanic, R. Discovery of a pair of very metal-poor stars enriched in neutron-capture elements: The proto-disk r-II star BPS CS 29529-0089 and the Gaia-Sausage-Enceladus r-I star TYC 9219-2422-1. *Astron. Astrophys.* **2025**, *696*, A122. https://doi.org/10.1051/0004-6361/202453295.
30. Prantzos, N.; Abia, C.; Cristallo, S.; Limongi, M.; Chieffi, A. Chemical evolution with rotating massive star yields II: A new assessment of the solar s- and r-process components. *Mon. Not. R. Astron. Soc.* **2020**, *491*, 1832–1850. https://doi.org/10.1093/mnras/stz3154.
31. Asplund, M.; Amarsi, A.M.; Grevesse, N. The chemical make-up of the Sun: A 2020 vision. *Astron. Astrophys.* **2021**, *653*, A141. https://doi.org/10.1051/0004-6361/202140445.
32. Cseh, B.; Világos, B.; Roriz, M.P.; Pereira, C.B.; D'Orazi, V.; Karakas, A.I.; Soós, B.; Drake, N.A.; Junqueira, S.; Lugaro, M. Barium stars as tracers of s-process nucleosynthesis in AGB stars. I. 28 stars with independently derived AGB mass. *Astron. Astrophys.* **2022**, *660*, A128. https://doi.org/10.1051/0004-6361/202142468.
33. Hansen, T.T.; Holmbeck, E.M.; Beers, T.C.; Placco, V.M.; Roederer, I.U.; Frebel, A.; Sakari, C.M.; Simon, J.D.; Thompson, I.B. The R-process Alliance: First release from the southern search for r-process-enhanced stars in the Galactic halo. *Astrophys. J.* **2018**, *858*, 92. https://doi.org/10.3847/1538-4357/aabacc.